Sustainable Food Technology

ROYAL SOCIETY OF CHEMISTRY

PAPER

View Article Online
View Journal | View Issue

Cite this: *Sustainable Food Technol.*, 2025, **3**, 2158

Probing sustainable cross-linked quince seed mucilage–sodium alginate biocomposite hydrogels through the development of biodegradable films

Sabreena Yousuf,[a] Nusrat Jan,[b] Nadira Anjum,[b] B. N. Dar,[c] J. A. Rather[c] and Shrikant S. Maktedar *[a]

Biocomposite hydrogels based on quince seed mucilage (QSM) and sodium alginate (SA) incorporated with crosslinkers (ZnO, $CaCl_2$ and NC) were developed and characterized. Biocomposite hydrogels were characterized for their rheological, structural and thermal properties. Hydrogels with a QSM-to-SA ratio of 80 : 20 and $CaCl_2$ as a crosslinker agent exhibited more elastic character and stronger gelation, as revealed by rheological studies, and improved structural and thermal properties, as revealed by Fourier transform infrared spectroscopy and differential scanning calorimetry. Hydrogels were further used for the development of films. The prepared biocomposite films were characterised for thickness, tensile strength (TS), water vapour transmission rate (WVTR) and oxygen transmission rate (OTR), biodegradability, instrumental color and antimicrobial activity. Significantly higher TS and lower WVTR and OTR ($P \leq 0.05$) were observed in the biocomposite films with $CaCl_2$ as a crosslinker agent. Biocomposite films with NC as a crosslinker agent exhibited significantly higher instrumental color parameters. Films incorporated with NC showed lower biodegradation by the soil burial test. Films with ZnO as a crosslinker agent exhibited greater inhibitory effect against *Aspergillus niger* and *Rhizopus stolonifer*. Overall, biocomposite films with an 80 : 20 ratio of QSM to SA and $CaCl_2$ as a crosslinker agent as food packaging can provide better protection to extend the food shelf life.

Received 18th March 2025
Accepted 22nd August 2025

DOI: 10.1039/d5fb00095e

rsc.li/susfoodtech

Sustainability spotlight

Sustainability provides robust solutions towards everyday challenges in society without having any detrimental effects on the surrounding environment; hence, it is important for achieving SDGs. Presently, food-packaging materials are creating an extra burden on Earth due to their inherent toxicity and non-degradability, *viz.*, the average lifespan of plastic on Earth is several years. Therefore, to address this issue, in this study, bioinspired polymers such as quince seed mucilage and sodium alginate were used for the development of composite hydrogels with $CaCl_2$, nanoclay and ZnO as crosslinkers. Furthermore, the as-prepared biodegradable films were fully characterized with various parameters and studied with the help of rheology, thermal and spectroscopic investigations. This work highlights the importance of the UN sustainable development goals, such as good health and well-being (SDG 3) and industry, innovation and infrastructure (SDG 9).

1. Introduction

Quince seed mucilage (QSM) is generally recognised as safe and is inexpensive, non-toxic, biocompatible, renewable and biodegradable. These properties make it suitable for the preparation of biopolymer films.[1] The swelling and deswelling properties of QSM are primarily due to the polysaccharide glucuronoxylan.[2] Moreover, QSM has a greater molecular weight (9.61×10^6 g mol^{-1}) than some commercially available and most applicable gums like xanthan gum, guar gum and gellan gum.[3] The poor strength and barrier properties of films and coatings prepared using QSM limit its use in food packaging despite being an economic polymer with great water absorption capacity.[4] These drawbacks of QSM are overcome by blending it with other biopolymers like sodium alginate to prepare biocomposites.[5] Sodium alginate has been used as a blending of diverse biopolymers to tailor the properties of coatings/films.[6] It is a polysaccharide consisting of (1,4)-linked β-D -mannuronic acid units and α-L-guluronic acid units. Alginate is obtained commercially from seaweed and has gel forming properties, which increase its scope in the packaging of food.[5,7] Moreover, it has applications in various pharmaceutical as well as cosmetic industries.[8] However, the disadvantages like high water vapor and gas permeability, low mechanical strength and solubility

[a]*Materials Chemistry & Engineering Research Laboratory, Department of Chemistry, National Institute of Technology, Srinagar 190006, J & K, India*

[b]*Sher-e-Kashmir University of Agricultural Sciences and Technology, Kashmir, J & K, India*

[c]*Islamic University of Science and Technology, Awantipora, J & K, India. E-mail: shrikant@nitsri.ac.in*

limit its applications in biodegradable films.[5] These drawbacks are overcome by the addition of a number of components like other biopolymers,[9] plant extracts,[10] pure active ingredients[11] and crosslinker additives.[12]

Hydrogels are three-dimensional water-absorbable polymeric networks commonly employed in the medical and pharmaceutical field due to their resemblance to the extracellular matrix constituents.[13,14] Moreover, its non-toxic, inert and biocompatible nature ensures that it does not influence the metabolic processes of living organisms. Formulation of hydrogels mostly requires the addition of crosslinkers to prevent the solubilization of polymeric chains before use. More recently, several promising crosslinkers with improved biocompatibility, biodegradability, toxicity and aqueous solubility have been investigated.[15–18] Moreover, crosslinking agents have been incorporated in hydrogel formulations to enhance the tensile strength and attain desired drug release characteristics.[19,20] Hydrogels exhibit viscoelastic to elastic behavior due to the incorporation of crosslinkers between the polymeric chains.[21,22]

Films from synthetic polymers are common applied materials in food packaging. Nevertheless, the mass use of plastics results in waste that is stored for many years, leading to environmental pollution.[23] Moreover, various studies have found the apparent ill effects of plastics in various tissues and organs,[24] human cells[25] and marine organisms.[26] Scientists have also reported the occurrence of microplastics in human milk.[27] Therefore, researchers nowadays are focused more on smart biomaterials for packaging that are non-toxic, edible, and biodegradable and can serve as potential substitutes to the existing polymer plastics.[28] In this study, QSM and sodium alginate (SA)-based biocomposite polymers were enriched with crosslinkers like nanoclay, ZnO and $CaCl_2$ to form hydrogels. The hydrogels based on QSM and sodium–alginate incorporated with crosslinkers were then used for the development of a biocompatible film.

2. Materials and methods

2.1. Materials

Sodium alginate (91% purity), nanoclay and ZnO were purchased from Sigma-Aldrich Co. Ltd, (St. Louis, MO, USA), while glycerol and $CaCl_2$ were purchased from Hi-Media Pvt. Ltd (India). All other chemicals and reagents used in this study were of analytical grade, and were procured from standard commercial suppliers (Sigma-Aldrich and HiMedia).

2.2. Extraction of quince seed mucilage

Quince seeds were purchased from a local market at Shalimar Srinagar, Jammu and Kashmir (J&K), India. After manual cleaning of the seeds, the extraction of aqueous QSM from whole seeds was carried out in distilled water for 30 min at 40 °C to induce mucilage exudation. The ratio of water to seed was 25 : 1 (v/w). The water-seed slurry was agitated with an electric mixing paddle throughout the extraction period to remove the mucilage layer from the surface of the seed. The solutions were then filtered using a cotton cloth, and the collected mucilage was oven-dried at 45 °C ± 1 °C to a constant weight. The dried mucilage was then bottled and kept under a cool and dry atmosphere. The QSM yield was approximately (7%) on dry weight basis.

2.3. Formulation of QSM/sodium alginate hydrogels

QSM and SA powders were dissolved in distilled water with continuous stirring at 80 °C for 1 h with the addition of glycerol (2 mL) as a plasticizer. The suspension was ultra-sonicated to remove air bubbles. Finally, various additives like nanoclay, ZnO and $CaCl_2$ were added to the hydrogels of QSM and sodium alginate mixtures at constant concentrations (Table 1). The hydrogels were homogenized at 8000 rpm for 15 min using a high-speed IKA T18 digital Ultra-Turrax.

2.3.1. Characterization of hydrogels

2.3.1.1. Rheological studies. Rheological characterization of the composite hydrogels was performed using a rheometer (Anton Paar MCR-101) fitted with a cone and plate geometry (diameter of 25 cm with a cone angle of 1.998 °C) having a Peltier temperature control system with an accuracy of ±0.01 °C in accordance with the procedure of Afzal *et al.*[29] The tests were performed at room temperature. In amplitude sweep tests, determination of the linear viscoelastic (LVE) region of the composite hydrogels was done at a frequency of 1 Hz to perform all the measurements within this range. For the determination of the flow properties and viscoelastic behavior of the composite hydrogels, steady shear tests (r = 0.1–100 s^{-1}) and frequency sweep tests (r = 0.1–100 s^{-1}) were performed at a constant strain (1).

2.3.1.2. Attenuated total reflection-Fourier transform infrared spectroscopy (ATR-FTIR). Hydrogels were characterized using ATR-FTIR (CARY 630, Agilent Technologies, USA) at room temperature to determine the polymer interactions. An IR spectrum of the samples was obtained in the frequency range of 4000–400 cm^{-1}. The spectral resolution was 4 cm^{-1} and 32 scans were used. The IR spectrum of air was first determined under the same conditions, which was then automatically deducted from the IR spectra of the samples.

2.3.1.3. Thermal properties (differential scanning calorimeter). Determination of the thermal properties of QSM/sodium alginate hydrogels with crosslinkers was done by using a differential scanning calorimeter (DSC) (DSC-1 STAR System, Mettler-Toledo). A hydrogel sample of 3.5 mg was taken in an aluminum pan, followed by the addition of about 8 μl of deionized water. The aluminum pans carrying the sample were kept at room temperature overnight after sealing them hermetically. The samples were then heated at the rate of 10 °C min^{-1} in the range of 30 °C to 300 °C. The reference for the determination of the thermal properties was an empty aluminum pan.

2.4. Preparation of the biocomposite films

Preparation of the biocomposite films was done according to the method of Zhang *et al.*[18] with some modifications. The biocomposite films from different combinations of hydrogels

Table 1 QSM, sodium alginate and NC/ZnO/$CaCl_2$ film-forming solution compositions

Treatments	Quince seed mucilage (%)	Sodium alginate (%)	Crosslinker concentration (mg/50 mL of hydrogel)
QAH1-NC (QSM + SA + NC)	100	0	0
QAH1-ZnO (QSM + SA + ZnO)	100	0	0
QAH1-$CaCl_2$ (QSM + SA + $CaCl_2$)	100	0	0
QAH2-NC (QSM + SA + NC)	80	20	25
QAH2-ZnO (QSM + SA + ZnO)	80	20	25
QAH2-$CaCl_2$ (QSM + SA + $CaCl_2$)	80	20	25
QAH3-NC (QSM + SA + NC)	60	40	25
QAH3-ZnO (QSM + SA + ZnO)	60	40	25
QAH3-$CaCl_2$ (QSM + SA + $CaCl_2$)	60	40	25
QAH4-NC (QSM + SA + NC)	40	60	25
QAH4-ZnO (QSM + SA + ZnO)	40	60	25
QAH4-$CaCl_2$ (QSM + SA + $CaCl_2$)	40	60	25
QAH5-NC (QSM + SA + NC)	20	80	25
QAH5-ZnO (QSM + SA + ZnO)	20	80	25
QAH5-$CaCl_2$ (QSM + SA + $CaCl_2$)	20	80	25

were developed by solution casting method, followed by evaporation of the solvent. A known amount of hydrogel solution was poured into the Petri plates (made of polypropylene) and dried in an oven at 60 °C for 12 h, and then peeled from the plate and conditioned at 50% ± 1% relative humidity (RH) and 25 °C before analysis.

2.4.1. Characterization of the biocomposite films

2.4.1.1. Film thickness. The biocomposite films were first cut into small strips of size 1 × 6 cm. The thickness was then measured at different points by a handheld micrometre (YAMAYO Instruments).

2.4.1.2. Instrumental color (L, a* and b*).* A Hunter Lab colorimeter (Model SN3001476, Accuracy Micro-sensors, New York) was used to determine the L^*, a^* and b values of the biocomposite films. After placing the samples on the plate, their exposure at different places was recorded according to the CIE LAB system of color measurement. CIE Lab is a color space where L^* indicates lightness, a^* represents the red-green axis, and b^* represents the yellow–blue axis. This color system allows for quantitative evaluation of color differences in materials.

2.4.1.3. Water vapor transmission rate (WVTR) and WVP (water vapour permeability). The WVTR of the film samples was determined by using a Labthink W3/031 automated water vapor transmission tester and the ASTM (American Society for Testing and Materials) standard method E96-80 procedure. The RH and temperature were set to 90% and 38 °C, respectively. For the experiments, the continuous mode was chosen. Three specimens of each film were measured and the average value was reported. WVP was calculated by the following given equation:

$$\mathrm{WVP} = \frac{\mathrm{WVTR} \times \mathrm{thickness}}{\Delta P}$$

where WVTR is the water vapor transmission rate (g h^{-1} m^{-2}), thickness is the film thickness (mm), and ΔP is the water vapor partial pressure difference across the film (kPa).

2.4.1.4. Oxygen transmission rate (OTR). The OTR of the film samples was determined in accordance with ISO 15105 2/ASTM D3985 standard using an oxygen transmission rate test apparatus (Model, OX2/230; Lab-think Instruments Co., Ltd). Prior to measurements, the samples were conditioned for 24 hours. The diffusion cell was clamped with flat film samples. Then, pure oxygen (99.99%) was supplied into the diffusion cell chamber, and the carrier gas carried oxygen molecules that had permeated through the film to the interior chamber to the colorimetric sensor (N_2).

2.4.1.5. Tensile strength (TS). The tensile strength (MPa) and elongation at break film samples was determined at 25 °C with a texture analyser (TA. XT Plus Texture stable microsystem). Specimens were taken in dumbbell shapes for the analysis.

2.4.1.6. Biodegradability test of the biocomposite films. The biodegradability of the films was ascertained by burying the samples under soil and then monitoring the weight loss after regular intervals of time. The films were cut in pieces with a size of 5 × 2 cm. The pieces were then tied with a thread at one corner, followed by burying them about 2–3 cm under the soil surface. The soil was kept humid by sprinkling it with water once daily. The pre-weighed pieces of film were then removed from the soil at intervals of 20, 40, 60 and 90 days. The adhered soil particles were cleaned off by washing the films with distilled water. The samples were then dried at room temperature to constant weight. The equation given below was used for the calculation of weight loss:[30]

$$\text{Weight loss } \% = \frac{W_i - W_d}{W_i}$$

where W_i = initial weight of the specimen and W_d = dry weight of the specimen after degradation in soil.

2.4.1.7. Antimicrobial activity. To investigate the antimicrobial activity of the biocomposite films, two fungal strains *Rhizopus stolonifer* and *Aspergillus niger* were used in this study. The antimicrobial activity was examined by disc diffusion assay. The potato dextrose agar medium was prepared and sterilized by autoclaving for 30 min at 121 °C. The media was allowed to solidify after being transferred into the Petri plates. Fungal inoculation was carried out using a spore suspension prepared in sterile distilled water, adjusted to a concentration of

approximately 1×10^5 CFU mL^{-1}. The test microorganisms were then swabbed on the surface of the solidified media plates. The biocomposite film samples were punched to make discs (7 mm in diameter). The discs were inoculated on the Petri plates, which were then incubated at 37 °C for 48 h. After incubation, the diameter of microbial inhibition was measured in mm scale.[31]

2.5. Statistical analysis

One-way and two-way analysis of variance (ANOVA) was employed using SPSS software at 5% level of significance. The difference between means was determined using Duncan's multiple range test (DMRT). The data are presented as an average of triplicates.

3. Results and discussion

3.1. Characterization of hydrogels

3.1.1. Rheological studies. Frequency sweep tests of the hydrogels were performed between the angular frequency of 0.1 to 100 sec^{-1} (Fig. 1). The hydrogels exhibited significant variation in viscoelastic behaviour by changing the proportion of QSM and sodium alginate with constant concentrations of crosslinker agents (ZnO, $CaCl_2$ and NC). The storage modulus (G') was higher than the loss modulus (G'') ($G' > G''$) in hydrogels with $CaCl_2$ as the crosslinking agent, denoting a more elastic nature, followed by hydrogels with NC and ZnO as crosslinkers when a load was applied. Thus, the results indicated a more elastic response and solid-like behaviour in hydrogels with $CaCl_2$. This could be attributed to the stronger ionic interaction of the Ca^{2+} ions with polymer reactive groups or backbone, and consequently a stronger hydrogel.[32] A higher storage modulus (G') indicates a solid-like or elastic behaviour of hydrogels, which in turn indicates higher strength and mechanical rigidity.

As can be observed from the results, hydrogels with an 80% concentration of sodium alginate and 20% QSM with ZnO, $CaCl_2$ and NC as crosslinkers exhibited a lower storage modulus (G'). However, increasing the concentration of QSM up to 80% and decreasing alginate resulted in a higher storage modulus (G'), indicating the dominance of the elastic behaviour on application of the load. Thus, the storage modulus (G') improves more quickly than the loss modulus (G'') when the concentration of QSM is increased and alginate is decreased, indicating that the hydrogel phase has converted into a solid-like gel with supreme elastic behaviour. This might be due to a greater amount of three-dimensional cross-linked networks of hydrogels.[33] QSM at 80% concentration exhibited a higher cross-linking level. This could be attributed to the availability of more carboxylate groups for crosslinking with Ca^{2+}, resulting in strong hydrogen-bond interactions and greater stabilization of the calcium-induced gelation than at higher alginate concentration.[7] This improves the mechanical and viscoelastic gelation behaviour. Similar results were reported by Cuomo *et al.*,[34] who found that the storage modulus (G') showed a certain dependence in hydrogels with higher value at low alginate content in the hydrogels.

The apparent viscosity curves of the QSM-alginate hydrogels incorporated with ZnO, $CaCl_2$ and NC as crosslinking agents are shown in Fig. 2. The steady-state flow of the QSM-alginate hydrogels demonstrate that all of the hydrogels showed shear rate ($\dot{\gamma}$) dependence and shear thinning behaviour. Thus, all hydrogels exhibited low viscosity as the shear rate increased from 0 to 100 1 S^{-1}. It was observed that the hydrogels immediately recovered into solid-like materials as the shear rate approached 0. Depending on the type of crosslinker agent, results showed that hydrogels with added $CaCl_2$ exhibited higher viscosity due to strong gelation. The shear rate of these hydrogels approached zero, indicating that the gel does not flow at rest. Moreover, hydrogels with NC as the crosslinker agent exhibited stronger gelation than hydrogels with ZnO, as revealed from the steady-state flow behaviour. Thus, the data indicate that hydrogels with $CaCl_2$ as the crosslinker constitutes the strong gel network.[7] Hydrogels with 80% concentration of QSM and 20% sodium alginate added with ZnO, $CaCl_2$ and NC as crosslinking agents showed higher viscosity values as the shear rate increases; thus, exhibiting stronger gelation followed by hydrogels formulated from pure QSM, which was independent of the specific shear rate and duration. Furthermore, the increase in the concentration of alginate from 20% to 80%

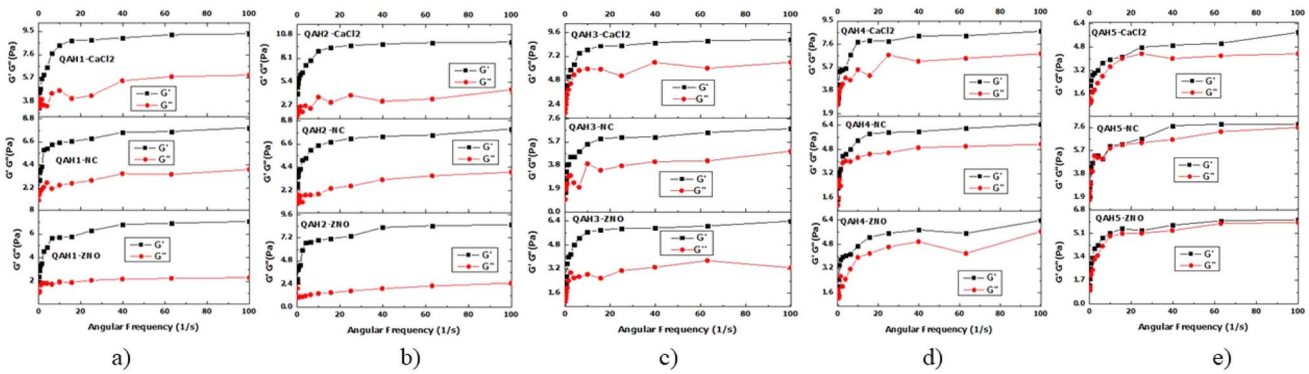

Fig. 1 (a–e) Frequency sweep test of QSM/sodium alginate hydrogels with different QSM : SA ratios (a) QAH1 (100 : 0), (b) QAH2 (80 : 20), (c) QAH3 (60 : 40), (d) QAH4 (40 : 60), (e) QAH5 (20 : 80), each crosslinked with $CaCl_2$, NC and ZnO.

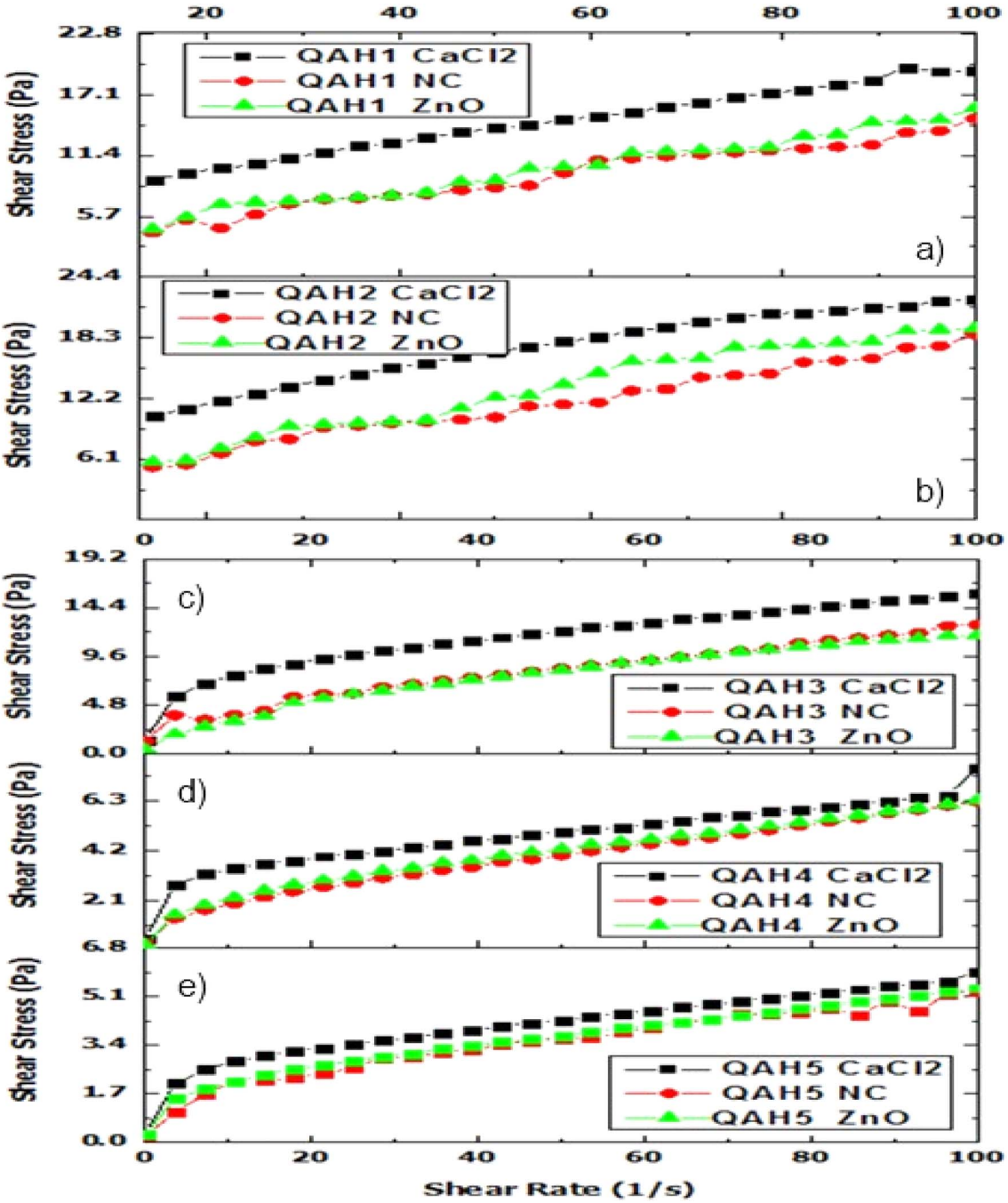

Fig. 2 Apparent viscosity curves of the QSM/alginate hydrogels with different QSM : SA ratios (a) QAH1 (100 : 0), (b) QAH2 (80 : 20), (c) QAH3 (60 : 40), (d) QAH4 (40 : 60), (e) QAH5 (20 : 80), with constant concentration of $CaCl_2$, NC and ZnO as crosslinker agents.

showed lower viscosity values, resulting in weaker gelation. Thus, the results concluded that hydrogels with a higher concentration of sodium alginate have more shear thinning properties compared to hydrogels with QSM. While comparing the crosslinking agents used, ZnO exhibited more shear thinning properties, followed by NC and $CaCl_2$. The notable shear-thinning behavior of the hydrogels suggests excellent processability for film production, as viscosity decreases under applied stress during casting or extrusion, enabling smoother, more uniform film formation while minimizing energy input. Additionally, a higher elastic modulus within the linear viscoelastic region supports structural integrity during drying and handling, which is critical for the scalable manufacturing of biodegradable films.

3.1.2. Attenuated total reflection-Fourier transform infrared spectroscopy (ATR-FTIR). ATR-FTIR spectroscopy was used to characterize hydrogels with varying concentrations of QSM and sodium alginate and with ZnO, $CaCl_2$ and NC as crosslinking agents, and Fig. 3 shows the spectral differences acquired from 4000 to 400 cm^{-1}. The FTIR spectra of hydrogels

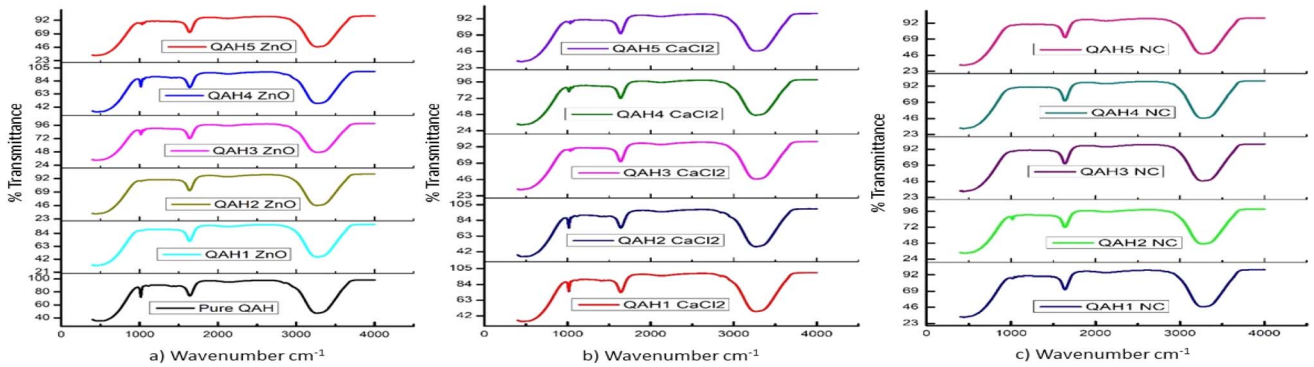

Fig. 3 FTIR spectra of the QSM/alginate hydrogels with constant concentration of ZnO, $CaCl_2$ and NC as crosslinker agents, with different QSM : SA ratios (a) QAH1-5 cross-linked with ZnO (b) QAH1-5 cross-linked with $CaCl_2$ (c) QAH1-5 cross-linked with NC.

crosslinked with ZnO revealed spectroscopic bands at 1554–1630 cm^{-1}, hydrogels crosslinked with $CaCl_2$ at 1559–1655 cm^{-1} and hydrogels crosslinked with NC at 1555–1651 cm^{-1}, which were related to the asymmetric and symmetric axial deformations of the $-COO^-$ groups.[35] The strong bands of hydrogels with $CaCl_2$ as crosslinker agents could be beneficial to improve the physical performance of biopolymer films. The shift in peaks to higher wavenumbers upon the addition of crosslinking agents might be attributed to the bonding between $-COO^-$ groups and crosslinkers ZnO, $CaCl_2$ and NC, which forms a three-dimensional crosslinked network of hydrogels. Loria *et al.*[36] also found a shift of peaks (1621 and 1414 cm^{-1}) to higher wavenumbers on interaction of ions (Ca^{2+}) with anionic groups (COO^-). A similar shift was observed in the present study, where the majority of $-COO^-$ anionic groups were crosslinked at lower concentrations of sodium alginate with the constant concentration of crosslinker agents (25 mg/50 mL of hydrogel). The FTIR spectra revealed a wide band between 3288 and 3345 cm^{-1} in QSM hydrogels crosslinked with ZnO, 3308 and 3680 cm^{-1} in those crosslinked with $CaCl_2$, and 3306 and 3500 cm^{-1} in those crosslinked with NC, corresponding to the stretching of the –OH groups present in the QSM and sodium alginate polymer chains.[37]

QSM hydrogels containing NC as a crosslinker showed a shift of peaks to higher wavenumbers, which might be due to the elongation of the –OH groups. The change was confirmed by the slight upward shift of the band.[38] The strong absorption bands were observed at 1106–1400 cm^{-1} for hydrogels with ZnO as the crosslinker agent, 1124–1401 cm^{-1} with NC as the crosslinker agent, and 1138 to 1407 cm^{-1} for hydrogels crosslinked with $CaCl_2$, corresponding to the C–O–C and C–O stretching vibrations.[39] Thus, the ATR-FTIR spectra confirmed that the $CaCl_2$ crosslinker agent, followed by NC, had good biocompatibility in QSM and sodium alginate films.

3.1.3. Thermal properties (DSC). The thermal properties of QSM-sodium alginate hydrogels incorporated with ZnO, $CaCl_2$ and NC were determined to find out the thermal energy required to break the chemical bonds present in the hydrogels (Table 3). The hydrogels containing ZnO as a crosslinking agent exhibited exothermic peaks at 244.01 °C (QAH1-ZnO), 245.65 °C (QAH2-ZnO), 241.55 °C (QAH3-ZnO), 240.66 °C (QAH4-ZnO), and 240.33 °C (QAH5-ZnO). Before these temperatures are attained, an increase in temperature results in an absorption of heat by the hydrogels. After these temperatures are attained, the temperature increase breaks the bonds present in the gel, resulting in disintegration of the gel structure.[40,41] From the heat flow curves of hydrogels containing ZnO as the crosslinking agent, it was observed that a higher exothermic temperature was exhibited by QAH2-ZnO and the lowest temperature was seen with QAH5-ZnO treatment. When QSM-sodium alginate hydrogels with a constant concentration of $CaCl_2$ as the crosslinker absorbed the heat, exothermic peaks were observed at 246.32 °C (QAH1-$CaCl_2$), 248.22 °C (QAH2-$CaCl_2$), 245.22 °C (QAH3-$CaCl_2$), 244.21 °C (QAH4-$CaCl_2$), and 243.17 °C (QAH5-$CaCl_2$). From the heat flow curves, it was observed that a higher exothermic temperature was exhibited by QAH2-$CaCl_2$ and the lowest temperature was seen with QAH5-$CaCl_2$ treatment. When QSM-sodium alginate hydrogels with a constant concentration of NC as the crosslinker agent absorbed the heat, exothermic peaks were observed at 243.12 °C (QAH1-NC), 244.33 °C (QAH2-NC), 243.07 °C (QAH3-NC), 242.78 °C (QAH4-NC), and 241.03 °C (QAH5-NC). From the heat flow curves, it was observed that a higher exothermic temperature was exhibited by QAH2-NC and the lowest temperature was seen with QAH5-NC treatment. Overall, the results showed that higher exothermic peaks were observed in hydrogels with $CaCl_2$ as the crosslinker agent. This could be attributed to the strong interactions between the Ca^{2+} ions of $CaCl_2$ and the polymer matrices in the hydrogels. However, in comparing the different biopolymer combinations, hydrogels with an 80% : 20% concentration of QSM and sodium alginate exhibited higher exothermic peaks, while hydrogels with a 20% : 80% concentration of QSM and sodium alginate showed lower peaks. This might be attributed to the increased entanglement of polymer chains and crosslinking, leading to increased hydrophobic interactions and thus resulting in higher exothermic peaks.[38] The thermal transitions observed by DSC are critical for defining the processing conditions and final film performance. Higher degradation onset temperatures ensure thermal stability during film casting, drying, and application in food packaging. These thermal properties therefore support scalable manufacturing, and ensure that the

developed biodegradable films maintain their mechanical and barrier functions under typical handling and storage conditions.

3.2. Characterization of the biocomposite films

3.2.1. Film thickness. The thickness of QSM and sodium alginate-based biocomposite films with added ZnO, $CaCl_2$ and NC as crosslinking agents is presented in Table 2. The thickness of the biocomposite films varied from 110.38 to 114.32 μm. It was observed that an increase in the sodium alginate concentration increased the thickness of the film. Significantly, the highest thickness was observed in biocomposite films with 20% : 80% concentration of QSM and sodium alginate ($P \leq 0.05$). The biocomposite films with higher QSM and lower alginate concentration exhibited lower value of thickness. This lower value of thickness might be due to the greater amount of three-dimensional cross-linked networks in the biocomposite films associated with the compact structure of the films.[6] Similar variations in film thickness based on biopolymer difference were observed by earlier research studies.[42,43] The type of crosslinker agent used showed a non-significant variation in the thickness of the biocomposite films among various treatments ($P \geq 0.05$).

3.2.2. Tensile strength (TS) and elongation break of biocomposite films. The tensile strength (TS) and elongation at break (EB) of QSM and sodium alginate-based biocomposite films are presented in Table 2. Significant difference ($P \leq 0.05$) was observed in the tensile strength and elongation at break, depending on the type of crosslinking agent and the QSM : sodium alginate ratio. Films crosslinked with $CaCl_2$ exhibited the highest TS and elongation at break values. The interfacial interaction among Ca^{2+} ions and polymer matrices is the main reason for the higher tensile strength of the biocomposite films. Moreover, the Ca^{2+} ions of $CaCl_2$ are positively charged, and are involved in electrostatic interaction with the negatively charged groups of the polymer matrix. This interaction could also contribute to the increased tensile strength.[44] NC-crosslinked films showed moderate TS and EB. This is likely due to interfacial reinforcement and the layered dispersion of nanoclay within the matrix, which promotes stress distribution while maintaining structural cohesion.[45] In contrast, ZnO-crosslinked films exhibited lower TS and the least elongation. This is possibly due to their rigid, aggregated structures restricting polymer chain mobility. Among the different biopolymer combinations, films prepared with a QSM : sodium alginate ratio of 80% : 20% demonstrated superior mechanical properties, achieving the highest TS and EB, followed by 100% QSM, 60% : 40%, 40% : 60% and 20% : 80%. The mechanical properties of the film depend on the microstructure and intermolecular forces of the polymer matrix. The variation in TS and EB with increasing concentration of sodium alginate in the biopolymer combination might be due to the weak intermolecular interactions, leading to structural discontinuity.[46] The higher TS and EB of pure QSM films than those of QSM films with a higher concentration of sodium alginate could be due to the compact structure and development of strong hydrogen bonds within the polymer matrix of pure QSM.

3.2.3. Barrier properties (WVTR and OTR) of biocomposite films. The barrier properties are considered an important parameter of films for application in food products. Table 2 shows the effect of crosslinking agents on WVTR of biocomposite films prepared with varying concentration of QSM and sodium alginate. Biocomposite films with $CaCl_2$ as the crosslinker exhibited significantly lower WVTR, while films with

Table 2 Thickness, TS, WVTR, WVP, EB and OTR of QSM/sodium alginate biocomposite films with NC/ZnO/$CaCl_2$ as crosslinker agents[a,b]

Treatments	Thickness (μm)	Tensile strength (MPa)	Elongation at break (%)	WVTR (g per m^2 per day)	WVP g m per m^2 per day per Pa	OTR (cm^3 per m^2 per day)
QAH1-NC	110.85 ± 0.23^{a}	33.37 ± 0.43^{e}	37.35 ± 0.32^{d}	306.17 ± 1.09^{c}	$6.04 \times 10^{-4} \pm 0.19^{a}$	1017.10 ± 2.23^{c}
QAH1-ZnO	110.33 ± 0.19^{a}	32.80 ± 0.27^{d}	35.26 ± 0.23^{cd}	335.11 ± 1.23^{f}	$6.58 \times 10^{-4} \pm 0.23^{c}$	1028.66 ± 1.88^{d}
QAH1-$CaCl_2$	110.22 ± 0.41^{a}	34.55 ± 0.33^{f}	40.12 ± 0.36^{f}	301.48 ± 1.33^{b}	$5.92 \times 10^{-4} \pm 0.37^{a}$	1009.11 ± 1.65^{b}
QAH2-NC	110.56 ± 0.33^{a}	34.83 ± 0.27^{f}	42.23 ± 0.41^{f}	306.14 ± 0.98^{c}	$6.03 \times 10^{-4} \pm 0.16^{a}$	1016.25 ± 2.34^{c}
QAH2-ZnO	110.54 ± 0.28^{a}	32.95 ± 0.21^{d}	36.12 ± 0.29^{d}	335.55 ± 1.22^{f}	$6.60 \times 10^{-4} \pm 0.28^{c}$	1029.70 ± 2.45^{d}
QAH2-$CaCl_2$	110.60 ± 0.44^{a}	36.12 ± 0.39^{g}	44.05 ± 0.13^{g}	299.72 ± 1.11^{a}	$5.90 \times 10^{-4} \pm 0.29^{a}$	1003.22 ± 2.01^{a}
QAH3-NC	110.38 ± 0.31^{a}	30.22 ± 0.58^{b}	34.26 ± 0.54^{c}	306.67 ± 1.14^{c}	$6.02 \times 10^{-4} \pm 0.41^{a}$	1042.26 ± 1.76^{ef}
QAH3-ZnO	110.41 ± 0.26^{a}	28.45 ± 0.36^{a}	38.02 ± 0.28^{e}	$336.47 \pm f0.86^{g}$	$6.61 \times 10^{-4} \pm 0.35^{c}$	1049.77 ± 2.09^{h}
QAH3-$CaCl_2$	111.44 ± 0.18^{ab}	32.12 ± 0.41^{c}	41.11 ± 0.62	303.50 ± 1.29^{b}	$6.02 \times 10^{-4} \pm 0.32^{a}$	1031.33 ± 2.20^{d}
QAH4-NC	111.15 ± 0.45^{ab}	29.40 ± 0.85^{b}	30.07 ± 0.36^{b}	308.45 ± 0.96^{cd}	$6.11 \times 10^{-4} \pm 0.15^{ab}$	1045.23 ± 2.04^{g}
QAH4-ZnO	112.22 ± 0.52^{ab}	27.44 ± 0.33^{a}	28.62 ± 0.38^{a}	337.12 ± 1.22^{g}	$6.74 \times 10^{-4} \pm 0.07^{d}$	1049.88 ± 1.67^{h}
QAH4-$CaCl_2$	113.05 ± 0.33^{ab}	31.39 ± 0.57^{bc}	33.25 ± 0.45^{c}	303.41 ± 0.83^{b}	$6.12 \times 10^{-4} \pm 0.11^{ab}$	1038.33 ± 2.04^{e}
QAH5-NC	113.35 ± 0.22^{c}	30.31 ± 0.76^{b}	28.03 ± 0.11^{a}	314.55 ± 1.11^{e}	$6.34 \times 10^{-4} \pm 0.34^{b}$	1058.25 ± 2.22^{i}
QAH5-ZnO	113.33 ± 0.46^{c}	27.02 ± 0.29^{a}	29.12 ± 0.26^{a}	338.49 ± 1.09^{g}	$6.82 \times 10^{-4} \pm 0.18^{e}$	1069.33 ± 2.41^{j}
QAH5-$CaCl_2$	114.32 ± 0.42^{c}	32.04 ± 0.24^{c}	34.17 ± 0.39^{c}	309.45 ± 0.93^{d}	$6.30 \times 10^{-4} \pm 0.06^{b}$	1044.22 ± 1.87^{g}

[a] All values are mean ± SD of three replicates. [b] Different letters in the same column indicate significant differences ($p < 0.05$).

Table 3 DSC data, instrumental color and antimicrobial activity of QSM/sodium alginate biocomposite films with NC/ZnO/$CaCl_2$ as crosslinker agents[a,b]

	DSC data		Instrumental color			Antimicrobial activity	
Treatments	Endothermic peak °C	Exothermic peak °C	L^*	a^*	b^*	Inhibition zone-diameter (mm) (*Aspergillus niger*)	Inhibition zone-diameter (mm) (*Rhizopus stolonifer*)
QAH1-NC	127.22 ± 2.30^{b}	243.12 ± 1.54^{c}	88.51 ± 1.23^{c}	-0.59 ± 0.07^{a}	5.99 ± 0.10^{b}	13.16 ± 0.03^{a}	10.04 ± 0.04^{a}
QAH1-ZnO	126.05 ± 1.09^{ab}	244.01 ± 1.37^{cd}	86.44 ± 0.98^{a}	-0.53 ± 0.06^{b}	4.32 ± 0.14^{a}	15.29 ± 0.04^{b}	12.32 ± 0.03^{b}
QAH1-$CaCl_2$	137.17 ± 1.13^{c}	246.32 ± 2.01^{d}	86.32 ± 1.11^{a}	-0.52 ± 0.03^{b}	4.98 ± 0.11^{a}	13.18 ± 0.04^{a}	10.34 ± 0.07^{a}
QAH2-NC	127.55 ± 2.02^{b}	244.33 ± 1.69^{cd}	88.89 ± 0.87^{c}	-0.58 ± 0.03^{a}	6.03 ± 0.17^{b}	13.21 ± 0.07^{a}	10.56 ± 0.03^{a}
QAH2-ZnO	126.32 ± 1.87^{ab}	245.65 ± 1.11^{d}	87.81 ± 1.14^{ab}	-0.51 ± 0.07^{b}	4.33 ± 0.15^{a}	15.83 ± 0.05^{b}	12.61 ± 0.04^{b}
QAH2-$CaCl_2$	137.33 ± 1.19^{c}	248.22 ± 2.20^{e}	87.80 ± 1.10^{ab}	-0.55 ± 0.08^{b}	4.12 ± 0.14^{a}	13.44 ± 0.03^{a}	10.65 ± 0.07^{a}
QAH3-NC	126.22 ± 1.54^{ab}	243.07 ± 2.03^{c}	88.22 ± 1.23^{c}	-0.58 ± 0.03^{a}	5.93 ± 0.09^{b}	13.55 ± 0.07^{a}	10.57 ± 0.07^{a}
QAH3-ZnO	126.07 ± 1.33^{ab}	241.55 ± 1.47^{a}	87.25 ± 1.09^{ab}	-0.53 ± 0.07^{b}	4.21 ± 0.11^{a}	15.82 ± 0.08^{b}	12.67 ± 0.04^{b}
QAH3-$CaCl_2$	137.22 ± 1.07^{c}	245.22 ± 1.44^{d}	87.13 ± 0.97^{ab}	-0.52 ± 0.10^{b}	4.22 ± 0.17^{a}	13.24 ± 0.05^{a}	10.55 ± 0.07^{a}
QAH4-NC	127.65 ± 2.01^{b}	242.78 ± 1.86^{ab}	88.42 ± 0.87^{c}	-0.57 ± 0.09^{a}	6.20 ± 0.13^{b}	15.83 ± 0.07^{a}	10.60 ± 0.06^{a}
QAH4-ZnO	124.33 ± 1.25^{a}	240.66 ± 2.01^{a}	87.11 ± 1.11^{ab}	-0.50 ± 0.07^{b}	4.77 ± 0.07^{a}	15.88 ± 0.08^{b}	12.62 ± 0.02^{b}
QAH4-$CaCl_2$	137.01 ± 1.44^{c}	244.21 ± 2.12^{cd}	87.33 ± 1.11^{ab}	-0.51 ± 0.04^{b}	4.66 ± 0.15^{a}	13.03 ± 0.04^{a}	10.44 ± 0.07^{a}
QAH5-NC	125.33 ± 1.83^{a}	241.03 ± 1.34^{a}	88.33 ± 0.86^{c}	-0.60 ± 0.02^{a}	5.97 ± 0.09^{b}	13.87 ± 0.07^{a}	10.63 ± 0.04^{a}
QAH5-ZnO	124.03 ± 1.79^{a}	240.33 ± 1.88^{a}	87.42 ± 1.14^{ab}	-0.51 ± 0.06^{b}	4.32 ± 0.16^{a}	15.84 ± 0.08^{b}	12.65 ± 0.03^{b}
QAH5-$CaCl_2$	137.11 ± 1.46^{c}	243.17 ± 1.62^{c}	87.32 ± 1.10^{ab}	-0.52 ± 0.09^{b}	4.33 ± 0.11^{a}	13.85 ± 0.02^{a}	10.66 ± 0.04^{a}

[a] All values are mean ± SD of three replicates. [b] Means with different superscripts (lowercase) in the same row differ significantly ($p < 0.05$).

ZnO as the crosslinker exhibited higher WVTR ($P \leq 0.05$). Similarly, the OTR was significantly lowest in films with $CaCl_2$ as the crosslinker and highest in films with ZnO as the crosslinker ($P \leq 0.05$). This might be attributed to the strong interactions among Ca^{2+} ions of $CaCl_2$ and polymer matrices in the films. After adding $CaCl_2$ to the biocomposite suspension, a dense microstructure might be formed, which enhanced the barrier properties of the developed biocomposite films. Furthermore, the addition of $CaCl_2$ to the biopolymer leads to the formation of egg-box like structures, which results in a zigzag path for water vapour and oxygen movement through the biocomposite film, thus reducing their diffusion.[47] Similarly, films crosslinked with $CaCl_2$ exhibited significantly lower water vapour permeability (WVP) values (*e.g.*, 5.92×10^{-4} to 6.12×10^{-4} g mm m^{-2} h^{-1} Pa^{-1}), suggesting improved moisture barrier properties. Conversely, ZnO-crosslinked films demonstrated higher WVP (*e.g.*, 6.58×10^{-4} to 6.82×10^{-4} g mm m^{-2} h^{-1} Pa^{-1}), consistent with the WVTR and OTR trends. These results suggest that stronger crosslinking leads to a tighter polymer matrix, restricting moisture transmission. However, the different biopolymer combinations films with 80% : 20% concentrations of QSM and sodium alginate

Table 4 Biodegradability (%) of QSM/sodium alginate biocomposite films with NC/ZnO/$CaCl_2$ as crosslinker agents[a,b]

	Biodegradability (%)			
Treatments	20th day	40th day	60th day	90th day
QAH1-NC	29.85 ± 0.21^{aA}	60.12 ± 0.54^{aB}	80.22 ± 0.83^{aC}	91.23 ± 1.12^{aD}
QAH1-ZnO	33.30 ± 0.37^{cA}	64.66 ± 0.66^{bBc}	84.32 ± 0.67^{cC}	94.42 ± 1.10^{bcD}
QAH1-$CaCl_2$	33.44 ± 0.19^{cA}	63.93 ± 0.51^{bB}	83.22 ± 0.92^{bC}	93.22 ± 0.96^{bD}
QAH2-NC	31.12 ± 0.27^{bA}	60.23 ± 0.46^{aB}	80.12 ± 0.76^{aC}	91.34 ± 0.87^{aD}
QAH2-ZnO	32.16 ± 0.31^{cA}	64.33 ± 0.39^{bcB}	84.54 ± 0.88^{cC}	94.82 ± 1.24^{bcD}
QAH2-$CaCl_2$	33.30 ± 0.41^{cA}	63.54 ± 0.47^{bB}	83.22 ± 0.93^{bC}	93.08 ± 1.11^{bD}
QAH3-NC	31.29 ± 0.21^{bA}	60.46 ± 0.56^{aB}	80.37 ± 0.57^{aC}	91.55 ± 0.98^{aD}
QAH3-ZnO	34.47 ± 0.40^{dA}	66.97 ± 0.44^{eB}	86.11 ± 1.01^{dC}	95.33 ± 0.75^{dD}
QAH3-$CaCl_2$	33.54 ± 0.18^{cA}	65.22 ± 0.37^{dB}	84.10 ± 0.67^{cC}	93.78 ± 0.10^{bcD}
QAH4-NC	31.62 ± 0.33^{bA}	61.14 ± 0.52^{bB}	80.53 ± 0.49^{aC}	92.10 ± 1.16^{abD}
QAH4-ZnO	32.64 ± 0.22^{cA}	67.45 ± 0.66^{eB}	87.22 ± 0.71^{eC}	96.11 ± 0.76^{eD}
QAH4-$CaCl_2$	33.22 ± 0.40^{cA}	66.30 ± 0.71^{eB}	84.33 ± 0.83^{cC}	95.22 ± 0.77^{dD}
QAH5-NC	32.10 ± 0.16^{bcA}	61.22 ± 0.53^{bB}	80.88 ± 0.77^{aC}	92.62 ± 0.86^{bD}
QAH5-ZnO	35.22 ± 0.22^{eA}	71.12 ± 0.47^{gB}	89.07 ± 0.93^{fC}	97.32 ± 1.04^{fD}
QAH5-$CaCl_2$	34.77 ± 0.31^{dA}	68.77 ± 0.63^{fB}	86.98 ± 0.87^{eC}	96.23 ± 1.01^{eD}

[a] All values are mean ± SD of three replicates. [b] Means in the same column with different superscripts (uppercase) differ significantly, and the means with different superscripts (lowercase) in the same row differ significantly ($p < 0.05$).

exhibited lower WVTR and OTR, followed by 100% QSM, 60% : 40%, 40% : 60% and 20% : 80%. The reason might be the hydrogen bonding and electrostatic interactions taking place due to the dense network arrangement within the polymer matrix, which enhances the water vapour and oxygen barrier capacity of the films. The increased concentration of sodium alginate caused discontinuity in the network structure, thus weakening the intermolecular interactions, which further results in an increase in the pore size, leading to an opportunity for water vapour and oxygen to diffuse though the films.[46] Similar trends in water vapor permeability (WVP) were also reported by Karambasti and Shavisi,[58] who developed guar gum–pectin nanofiber mats. Likewise, Heydarian and Shavisi[59] observed comparable WVP behavior in electrospun gelatin–xanthan gum mats containing chitin nanofibers and anthocyanins.

3.2.4. Biodegradability (%) of biocomposite films. The ability of biodegradable polymers to decompose by the action of microorganisms is their most significant advantage over petroleum-based plastics. According to Kochkina, and Lukin,[48] a bioplastic is considered to be biodegradable if it is degraded by 90% in 90 days. Table 4 depicts the influence of crosslinker agents and various combinations of QSM and sodium alginate on the biodegradability of biocomposite films using the soil burial test for 90 days. All treatments were almost destroyed at the 90th day of testing. However, the biocomposite films incorporated with NC as the crosslinker agent showed significantly less biodegradation compared to the other treatments after 90 days ($P \leq 0.05$). The water solubility of the biofilms is an important criterion for biodegradability because the penetration of soil moisture content in the polymer chains of biofilm weakens them and renders them susceptible to the action of microorganisms. The soil microorganisms hydrolyse the glycosidic linkages of the polymer, leading to its degradation.[30,49] Thus, on the basis of NC as an inorganic material that enhances the mechanical strength, the films incorporated with NC were stronger than the films with $CaCl_2$ and ZnO as crosslinking agents, which might have delayed the degradation rate. Shekarabi *et al.*[50] demonstrated that the incorporation of NC decreased the water solubility of QSM films. Slavutsky *et al.*[51] reported that films prepared by using 5% clay and starch exhibited a decrease in water solubility compared to the control without clay. The authors illustrated that this decrease could be due the interaction of clay with starch chains in the nanocomposite films. Ojagh *et al.*[43] observed similar results for methylcellulose films. Comparing the biofilms with different biopolymer combinations, films with 80% : 20% concentrations of QSM and sodium alginate exhibited lower biodegradability, followed by 100% QSM, 60 : 40%, 40 : 60% and 20 : 80% QSM and sodium alginate. The reason might be due to the strong intermolecular interactions and the enhanced mechanical properties of the biocomposite films.[52]

3.2.5. Instrumental color (L^*, a^*, and b^*) of biocomposite films. The results of the color parameters (L^*, a^* and b^*) of the biocomposite films are presented in Table 3. The films were homogeneous, uniform and transparent with a slight whitish tint. Biocomposite films with NC as the crosslinking agent exhibited significantly higher L^* and b^* values and lower a^* value ($P \leq 0.05$). However, the color parameters among films prepared with $CaCl_2$ and ZnO as the crosslinking agents exhibited non-significant variation ($P \geq 0.05$). The variation in L^* and b^* values of biofilms with NC as the crosslinker might be due to the increase in the reflection of light and subsequent decrease in the passage of light through films.[53] Abdollahi *et al.*[54] reported similar results of bionanocomposite films containing NC. Comparing the biocomposite films with different biopolymer combinations, a non-significant variation was observed among all of the color parameters ($P \geq 0.05$).

3.3. Antimicrobial activity of biocomposite films

Evaluation of the antimicrobial efficacy of the developed QSM and sodium alginate films with added ZnO, $CaCl_2$ and NC as crosslinking agents was assessed against *Aspergillus niger* and *Rhizopus stolonifer* (Table 3). The diameter of the inhibition zone indicated the inhibitory activity of the films. Biocomposite films incorporated with ZnO clearly showed a greater inhibitory effect against *Aspergillus niger* and *Rhizopus stolonifer* in comparison to films containing $CaCl_2$ and NC ($P \leq 0.05$). The exact mechanism of antimicrobial properties of ZnO is still not known. However, several authors have proposed that the release of Zn^{2+} ions, generation of reactive oxygen species (ROS) and physical interactions with the microorganisms are possible mechanisms in the inhibition of bacterial and fungal growth.[55] Earlier research studies also reported the antimicrobial properties of ZnO in packaging films.[56,57]

4. Conclusion

A novel biocomposite film was successfully developed based on QSM and sodium alginate, crosslinked with $CaCl_2$, ZnO, and NC. The films were characterized in terms of the thickness, tensile strength, WVTR, OTR, biodegradability, color (L^*, a^*, b^*), and antimicrobial activity, while the hydrogels were examined with rheology, ATR-FTIR, and DSC. Hydrogels with 80 : 20 QSM : sodium alginate crosslinked using $CaCl_2$ possessed better rheological properties, resulting in greater elastic behavior and higher gel network strength, followed by ZnO and NC. This was due to the three-dimensional crosslinked network resulting from hydrogen bonding and electrostatic interactions in the polymer matrices. Biocomposite films with a 20% : 80% ratio of QSM : sodium alginate exhibited the maximum film thickness, reflecting the enhanced film-forming ability. Meanwhile, the $CaCl_2$-crosslinked films exhibited much greater tensile strength, reflecting greater mechanical stability for future application in food protection. $CaCl_2$-crosslinked films also exhibited the minimum water vapor transmission rate (WVTR) and oxygen transmission rate (OTR), enhancing the barrier properties. NC-crosslinked films exhibited lower biodegradation in the 90-day soil burial testing compared to the other samples. ZnO-incorporated films had the maximum antimicrobial activity, making them suitable for active packaging. Overall, our findings determine that an 80% : 20% ratio of QSM to sodium alginate in biocomposite films exhibits

strong potential to be applied as a food packaging material to extend the shelf life of perishable food products.

Conflicts of interest

There are no conflicts to declare.

Data availability

The data used are provided in the manuscript.

References

1 S. A. Ghumman, A. Mahmood, S. Noreen, M. Rana, H. Hameed, B. Ijaz, S. Hasan, A. Aslam and M. F. Rehman, Formulation and evaluation of quince seeds mucilage – sodium alginate microspheres for sustained delivery of cefixime and its toxicological studies, *Arabian J. Chem.*, 2022, **15**, 103811.

2 B. Lindberg, M. Mosihuzzaman, N. Nahar, R. M. Abeysekera, R. G. Brown and J. M. Willison, An unusual (4-O-methyl-Dglucurono)-D-xylan isolated from the mucilage of seeds of the quince tree (*Cydonia oblonga*), *Carbohydr. Res.*, 1990, **207**, 307–310.

3 F. Rezagholi, S. M. B. Hashemi, A. Gholamhosseinpour, M. H. Sherahi, M. A. Hesarinejad and M. T. Ale, Characterizations and rheological study of the purified polysaccharide extracted from quince seeds, *J. Sci. Food Agric.*, 2019, **99**, 143–151.

4 S. Beikzadeh, A. Khezerlou, S. M. Jafari, Z. Pilevar and A. M. Mortazavian, Seed mucilages as the functional ingredients for biodegradable films and edible coatings in the food industry, *Adv. Colloid Interface Sci.*, 2020, **280**, 102164.

5 L. M. Júnior, E. Jamróz, S. A. Gonçalves, R. G. Silva, R. M. V. Alves and R. P. Vieira, Preparation and characterization of sodium alginate films with propolis extract and nano-SiO_2, *Food Hydrocolloids*, 2022, **2**, 100094.

6 S. A. Ghumman, S. Bashir, J. Ahmad, H. Hameed and I. U. Khan, Colocasia esculenta corms mucilage-alginate microspheres of oxcarbazepine: design, optimization and evaluation, *Acta Pol. Pharm.*, 2017, **74**, 505–517.

7 A. Manuja, B. Kumar, S. Athira, P. Sarkar, T. Riyesh, N. Kumar, B. N. Tripathi and B. Mann, Zinc oxide nanoparticles encapsulated in polysaccharides algi-nate/gum acacia and iron oxide nanomatrices show enhanced biocompatibility and permeability to intestinal barrier, *Food Hydrocolloids*, 2022, **2**, 100050.

8 S. Karmakar, S. Manna, S. Kabiraj and S. Jana, Recent progress in alginate-based carriers for ocular targeting of therapeutics, *Food Hydrocolloids*, 2022, **2**, 100071.

9 L. H. de Oliveira, P. Trigueiro, J. S. N. Souza, M. S. de Carvalho, J. A. Osajima, E. C. da Silva Filho and M. G. Fonseca, Montmorillonite with essential oils as antimicrobial agents, packaging, repellents, and insecticides: An overview, *Colloids Surf.*, 2022, **209**, 112186.

10 J. R. Nastasi, V. Kontogiorgos, V. D. Daygon and M. A. Fitzgerald, Pectin-based films and coatings with plant extracts as natural preservatives: A systematic review, *Trends Food Sci. Technol.*, 2022, **120**, 193–211.

11 G. A. Sutil, K. S. Andrade, E. A. Rebelatto and M. Lanza, Effects of incorporation of pure or multicomponent active agents in biopolymers for food packag-ing using supercritical CO2, *Trends Food Sci. Technol.*, 2022, **120**, 349–362.

12 R. Singh and V. Mahto, Synthesis, characterization and evaluation of polyacrylamide graft starch/clay nanocomposite hydrogel system for enhanced oil recovery, *Pet. Sci.*, 2017, **14**, 765–779.

13 K. Müller, E. Bugnicourt, M. Latorre, M. Jorda, Y. Echegoyen Sanz, J. M. Lagaron, O. Miesbauer, A. Bianchin, S. Hankin and U. Bölz, Review on the processing and properties of polymer nanocomposites and nanocoatings and their applications in the packaging, automotive and solar energy fields, *Nanomaterials*, 2017, **7**, 74.

14 S. M. Lee and D. Tiwari, Organo and inorgano-organo-modified clays in the remediation of aqueous solutions: An overview, *Appl. Clay Sci.*, 2012, **59**, 84–102.

15 M. R. Irshidat and M. H. Al-Saleh, Thermal performance and fire resistance of nanoclay modified cementitious materials, *Constr. Build. Mater.*, 2018, **159**, 213–219.

16 W. Janik, M. Nowotarski, D. Y. Shyntum, A. Banaś, K. Krukiewicz, S. Kudła and G. Dudek, Antibacterial and Biodegradable Polysaccharide-Based Films for Food Packaging Applications: Comparative Study, *Materials*, 2022, **15**, 3236.

17 M. Szekalska, K. Sosnowska, A. Czajkowska-Kośnik and K. Winnicka, Calcium chloride modified alginate microparticles formulated by the spray drying process: a strategy to prolong the release of freely soluble drugs, *Materials*, 2018, **11**, 1522.

18 Z. J. Zhang, N. Li, H. Z. Li, X. J. Li, J. M. Cao, G. P. Zhang and D. L. He, Preparation and characterization of biocomposite chitosan film containing *Perilla frutescens* (L.) Britt. essential oil, *Ind. Crops Prod.*, 2018, **112**, 660–667.

19 I. Kim, K. Viswanathan, G. Kasi, S. Thanakkasaranee, K. Sadeghi and J. Seo, ZnO nanostructures in active antibacterial food packaging: Preparation methods, antimicrobial mechanisms, safety issues, future prospects, and challenges, *Food Rev. Int.*, 2020, **38**, 537–565.

20 O. Oprea, E. Andronescu, D. Ficai, A. Ficai, F. Oktar and M. Yetmez, ZnO Applications and Challenges, *Curr. Org. Chem.*, 2014, **18**, 192–203, DOI: **10.2174/1385272813176660143**.

21 N. Jones, B. Ray, K. T. Ranjit and A. C. Manna, Antibacterial activity of ZnO nanoparticle suspensions on a broad spectrum of microorganisms, *FEMS Microbiol. Lett.*, 2008, **279**, 71–76.

22 A. Lipovsky, Y. Nitzan, A. Gedanken and R. Lubart, Antifungal activity of ZnO nanoparticles-The role of ROS mediated cell injury, *Nanotechnology*, 2011, **22**, 105101.

23 N. Zhang, F. Bi, F. Xu, H. Yong, Y. Bao and C. Jin, Structure and functional properties of active packaging films prepared

by incorporating different flavonols into chitosan based matrix, *Int. J. Biol. Macromol.*, 2020, **165**, 625–634.

24 K. Yin, Y. Wang, H. Zhao, D. Wang, M. Guo, M. Mu, Y. Liu, X. Nie, B. Li, J. Li and M. Xing, M, A comparative review of microplastics and nanoplastics: Toxicity hazards on digestive, reproductive and nervous system, *Sci. Total Environ.*, 2021, **7749**, 145758.

25 E. Danopoulos, M. Twiddy, R. West and J. M. Rotchell, A rapid review and meta regression analyses of the toxicological impacts of microplastic exposure in human cells, *J. Hazard. Mater.*, 2022, **427**, 127861.

26 Y. Han, F. Lian, Z. Xiao, S. Gu, X. Cao, Z. Wang and B. Xing Z, Potential toxicity of nanoplastics to fish and aquatic invertebrates: Current understanding, mechanistic interpretation, and meta-analysis, *J. Hazard. Mater.*, 2022, **427**, 127870.

27 A. Ragusa, V. Notarstefano, A. Svelato, A. Belloni, G. Gioacchini, C. Blondeel, E. Zucchelli, C. De Luca, S. D'Avino, A. Gulotta and O. Carnevali, O, Raman microspectroscopy detection and characterisation of microplastics in human breastmilk, *Polymers*, 2022, **14**, 2700.

28 Y. Wang, X. Wang, G. Hu, A. Al-Romaima, X. Liu, X. Bai, J. Li, Z. Li and M. Qui, Effect of green coffee oil as a natural active emulsifying agent on the properties of corn starch-based films, *LWT–Food Sci. Technol.*, 2022, **170**, 114087.

29 S. Afzal, M. Maswal and A. A. Dar, Rheological behavior of pH responsive composite hydrogels of chitosan and alginate: Characterization and its use in encapsulation of citral, *Colloids Surf., B*, 2018, **169**, 99–106.

30 K. S. Sarojini, M. P. Indumathi and G. R. Rajarajeswari, Mahua oil-based polyurethane/chitosan/nano ZnO composite films for biodegradable food packaging applications, *Int. J. Biol. Macromol.*, 2019, **124**, 163–174.

31 H. Palza, Antimicrobial Polymers with Metal Nanoparticles, *Int. J. Mol. Sci.*, 2015, **16**, 2099–2116.

32 A. Jastram, J. Claus, P. A. Janmey and U. Kragl, Rheological properties of hydrogels based on ionic liquids, *Polym. Test.*, 2021, **93**, 106943.

33 M. Ghanbari, A. Sadjadinia, N. Zahmatkesh, F. Mohandes, B. Dolatyar, B. Zeynali and M. Salavati-Niasari, Synthesis and investigation of physicochemical properties of alginate dialdehyde/gelatin/ZnO nanocomposites as injectable hydrogels, *Polym. Test.*, 2022, **110**, 107562.

34 F. Cuomo, M. Cofelice and F. Lopez F, Rheological characterization of hydrogels from alginate-based nanodispersion, *Polymers*, 2019, **11**(2), 259.

35 A. Omoike and J. Chorover, Spectroscopic study of extracellular polymeric substances from Bacillus subtilis: aqueous chemistry and adsorption effects, *Biomacromolecules*, 2004, **5**, 1219–1230.

36 K. G. Loria, A. M. R. Pilosof and M. E. Farías, M.E. Self-association of caseinomacropeptide in presence of $CaCl_2$ at neutral pH: Calcium binding determination, *LWT–Food Sci. Technol.*, 2022, **161**, 113419.

37 H. Hosseinzadeh and S. Mohammadi, Quince seed mucilage magnetic nanocomposites as novel bioadsorbents for efficient removal of cationic dyes from aqueous solutions, *Carbohydr. Polym.*, 2015, **134**, 213–221.

38 R. S. Fernandes, M. R. DeMoura, G. M. Glenn and F. A. Aouad, Thermal, microstructural, and spectroscopic analysis of Ca2+ alginate/clay nanocomposite hydrogel beads, *J. Mol. Liq.*, 2018, **265**, 327–336.

39 N. Cebi, Quantification of the geranium essential oil, palmarosa essential oil and phenylethyl alcohol in rosa damascena essential oil using ATR-FTIR spectroscopy combined with chemometrics, *Foods*, 2021, **10**, 1848.

40 Y. Liu, C. Dai, K. Wang, M. Zhao, G. Zhao, S. Yang, Z. Yan and Q. You, New insights into the hydroquinone (HQ)–hexamethylenetetramine (HMTA) gel system for water shut-off treatment in high temperature reservoirs, *J. Ind. Eng. Chem.*, 2016, **35**, 20–28.

41 G. Zhao, C. Dai, A. Chen, Z. Yan and M. Zhao, Experimental study and application of gels formed by nonionic polyacrylamide and phenolic resin for in-depth profile control, *J. Pet. Sci. Eng.*, 2015, **135**, 552–560.

42 L. Sun, J. Sun, L. Chen, P. Niu, X. Yang and Y. Guo, Preparation and characterization of chitosan film incorporated with thinned young apple polyphenols as an active packaging material, *Carbohydr. Polym.*, 2017, **163**, 81–91.

43 S. M. Ojagh, M. Rezaei, S. H. Razavi and S. H. S. Hoseini, Development and evaluation of a novel biodegradable film made from chitosan and cinnamon essential oil with low affinity toward water, *Food Chem.*, 2010, **122**, 161–166.

44 L. S. F. Leite, F. K. V. Moreira, L. H. C. Mattoso and J. Bras, Electrostatic interactions regulate the physical properties of gelatin-cellulose nanocrystals nanocomposite films intended for biodegradable packaging, *Food Hydrocolloids*, 2021, **113**(2021), 106424.

45 T. P. Mohan, K. Devchand and K. Kanny, Barrier and biodegradable properties of corn starch-derived biopolymer film filled with nanoclay fillers, *J. Plast. Film Sheeting*, 2017, **33**, 309–336.

46 T. Li, N. Xia, L. Xu, H. Zhang, H. Zhang, Y. Chi, Y. Zhang, L. Li and h. Li, Preparation, characterization and application of SPI-based blend film with antioxidant activity, *Food Packag. Shelf Life*, 2021, **27**, 100614.

47 B. Wang, S. Yan, W. Gao, X. Kang, B. Yu, P. Liu, L. Guo, B. Cui and A. M. Abd El- Aty, Antibacterial activity, optical, and functional properties of corn starch-based films impregnated with bamboo leaf volatile oil, *Food Chem.*, 2021, **357**, 129743.

48 N. E. Kochkina and N. D. Lukin, Structure and properties of biodegradable maize starch/chitosan composite films as affected by PVA additions, *Int. J. Biol. Macromol.*, 2020, **157**, 377–384.

49 K. M. S. Meera, R. M. Sankar, J. Paul, S. N. Jaisankar and A. B. Mandal, The influence of applied silica nanoparticles on a bio-renewable castor oil based polyurethane nanocomposite and its physicochemical properties, *Phys. Chem. Chem. Phys.*, 2014, **16**, 9276–9288.

50 A. S. Shekarabi, A. R. Oromiehie, A. Vaziri, M. Ardjmand and A. A. Safekordi, Investigation of the effect of nanoclay on the

properties of quince seed mucilage edible films, *Food Sci. Nutr.*, 2014, **2**(6), 821–827.

51 A. M. Slavutsky, M. A. Bertuzzi and M. Armada, Water barrier properties of starch-clay nanocomposite films, *Braz. J. Food Technol.*, 2012, **15**, 208–218.

52 L. Jiang, F. Wang, X. Xie, C. Xie, A. Li, N. Xia, X. Gong and H. Zhang, Development and characterization of chitosan/guar gum active packaging containing walnut green husk extract and its application on fresh-cut apple preservation, *Int. J. Biol. Macromol.*, 2022, **209**, 1307–1318.

53 S. B. Ghelejlu, M. Esmaiili and H. Almasi, Characterization of chitosan–nanoclay bio nanocomposite active films containing milk thistle extract, *Int. J. Biol. Macromol.*, 2021, **86**, 613–621.

54 M. Abdollahi, M. Rezaei and G. Farzi, A novel active bionanocomposite film incorporating rosemary essential oil and nanoclay into chitosan, *J. Food Eng.*, 2012, **111**, 343–350.

55 K. Vázquez, P. Vanegas, C. Cruzat, N. Novoa, R. Arrué and E. Vanegas, Antibacterial and antifungal properties of electrospun recycled PET polymeric fibers functionalized with zinc oxide nanoparticles, *Polymers*, 2021, **13**, 3763.

56 K. Y. Yoon, J. H. Byeon, J. H. Park and J. Hwang, J. Susceptibility constants of *Escherichia coli* and *Bacillus subtilis* to silver and copper nanoparticles, *Sci. Total Environ.*, 2017, **373**, 572–575.

57 A. Sirelkhatim, S. Mahmud, A. Seeni, N. H. M. Kaus, L. C. Ann, S. K. M. Bakhori, H. Hasan and D. Mohamad, Review on zinc oxide nanoparticles: antibacterial activity and toxicity mechanism, *Nano-Micro Lett.*, 2015, **7**, 219–242.

58 P. R. Karambasti and N. Shavisi, Development of guar gum-pectin nanofiber mats containing Papaver rhoeas petal anthocyanins and cellulose nanocrystals for real-time visual detection of lamb meat freshness, *LWT*, 2024, **194**, 115786.

59 A. Heydarian and N. Shavisi, Multifunctional food packaging materials: Electrospun mats based on gelatin-xanthan gum containing chitin nanofibers and black barberry anthocyanins for freshness monitoring and enhancing the shelf-life quality of Pacific white shrimps, *Food Packag. Shelf Life*, 2023, **40**, 101219.